Marangoni Bursting: Evaporation-Induced Emulsification of Binary Mixtures on a Liquid Layer

L. Keiser,[1,2] H. Bense,[1] P. Colinet,[3] J. Bico,[1,†] and E. Reyssat[1,*]
[1]Laboratoire de Physique et Mécanique des Milieux Hétérogènes (PMMH), CNRS, ESPCI Paris, PSL Research University, 10 rue Vauquelin, 75005 Paris, France and Sorbonne Universités, Université Paris Diderot
[2]Total S.A., Pôle d'Études et de Recherche de Lacq, BP47, 64170 Lacq, France
[3]Université Libre de Bruxelles, TIPs (Transfers, Interfaces and Processes), CP 165/67, Avenue F. D. Roosevelt 50, B-1050 Brussels, Belgium
(Received 24 November 2016; published 17 February 2017)

Adjusting the wetting properties of water through the addition of a miscible liquid is commonly used in a wide variety of industrial processes involving interfaces. We investigate experimentally the evolution of a drop of water and volatile alcohol deposited on a bath of oil: The drop spreads and spontaneously fragments into a myriad of minute droplets whose size strongly depends on the initial concentration of alcohol. Marangoni flows induced by the evaporation of alcohol play a key role in the overall phenomenon. The intricate coupling of hydrodynamics, wetting, and evaporation is well captured by analytical scaling laws. Our scenario is confirmed by experiments involving other combinations of liquids that also lead to this fascinating phenomenon.

DOI: 10.1103/PhysRevLett.118.074504

The fate of a droplet deposited on a substrate is of crucial importance for numerous applications ranging from coating processes to inkjet printing or phytosanitary treatments. Equilibrium values of surface tension classically dictate the wetting and wicking properties of liquids [1]. However, evaporation can also induce complex flows as illustrated by seminal works on coffee stains [2–8]. Evaporation causes variations in the temperature or the composition of liquids. Both effects result into local variations of the surface tension, which can in turn induce surface flows referred to as "Marangoni flows" after the pioneering work of Marangoni in the 1870s [9]. Besides explaining the self-propulsion of particles [10] or some insects [11] at the surface of water, Marangoni stresses can be used to manipulate droplets at small scales [12–16]. They also significantly affect the shape [17–19] and spreading dynamics of droplets [20–23] and often lead to intriguing fingering instabilities [24–30]. A popular and festive manifestation of these instabilities is the formation of "tears" along the walls of a glass of wine [31,32]. While the evaporation-induced flows of liquids lying on a solid substrate have been extensively studied, the evolution of an evaporating liquid on a nonmiscible fluid layer has only recently received attention [33,34].

In the present study, we focus on the instability observed when a two-component drop of water and volatile alcohol is deposited on a bath of sunflower oil. The drop temporarily spreads and spontaneously breaks up into thousands of tiny droplets [Fig. 1(a)]. We demonstrate experimentally how this spreading and fragmentation instability result from the interplay of a wetting transition at the contact line and solutal Marangoni effects, both induced by the fast evaporation of alcohol.

A millimetric drop of a mixture composed of water and isopropyl alcohol (IPA) is gently deposited on a centimeter-thick layer of sunflower oil. Provided the initial mass fraction ϕ_0 of IPA in the drop is sufficiently high, the drop spreads and reaches a nearly steady centimetric radius within a few seconds [Fig. 1(a) and Supplemental Movies 1–4 [35]]. The system, sketched in Fig. 1(b), is, however, not at rest as revealed by the myriad of submillimetric droplets continuously released from the periphery of the mother drop. The time evolution of the radius of the drop $R(t)$ [defined in Figs. 1(a) and 1(b)] is plotted in Fig. 1(c) for various experimental conditions. Once the drop has reached its maximal radius $R_{\max}$, its border starts to recede while keeping ejecting droplets. The phenomenon ends after a time $t_{\exp}$, once the initial drop has been totally fragmented.

The initial concentration of IPA ϕ_0 is a key parameter in this experiment. Indeed, we observe the instability only if ϕ_0 is above a critical value $\phi_c = 0.35 \pm 0.02$. For $\phi_0 < \phi_c$, a quasisteady drop simply sits at the surface of the oil and progressively decreases in size as the alcohol evaporates. The remaining water evaporates on a much longer time scale of tens of minutes. To interpret the onset of instability, we measured the interfacial tensions γ_{oa}, γ_{ma}, and γ_{mo} of the respective oil-air, mixture-air, and mixture-oil interfaces. Figure 2 shows the variations of these interfacial tensions with ϕ_0. The drop is expected to spread on oil for positive values of the spreading parameter $S = \gamma_{\mathrm{oa}} - \gamma_{\mathrm{ma}} - \gamma_{\mathrm{mo}}$ [1]. This criterion is found to coincide with the onset of the instability, which is confirmed by additional experiments using ethanol-water mixtures (see Sec. II in Supplemental Material [35]). A necessary condition to observe the instability is therefore that the initial mixture completely wets the supporting oil bath.

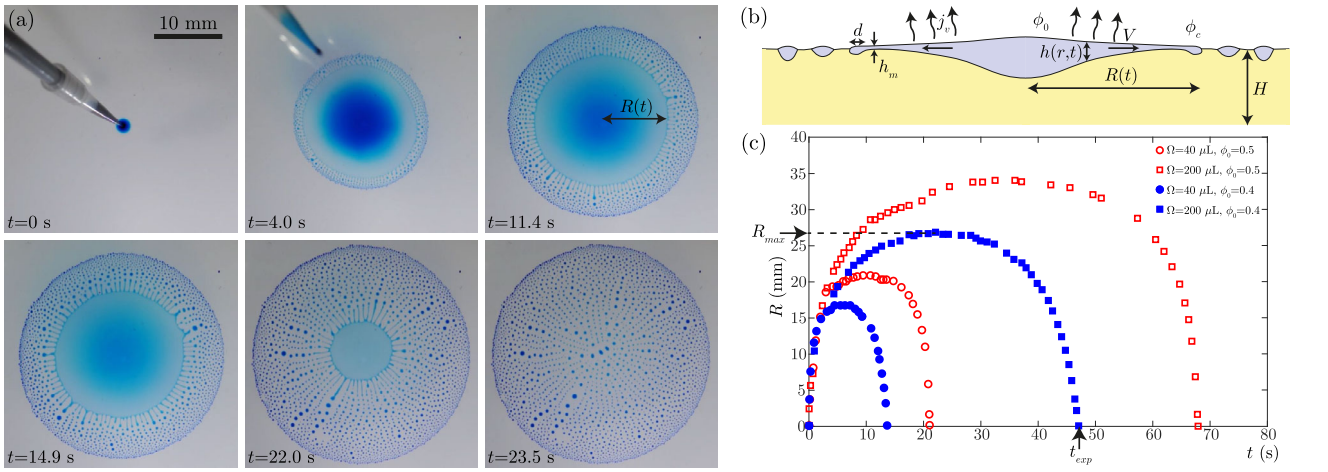

FIG. 1. (a) Image sequence of a drop of a mixture of isopropyl alcohol (IPA) with water spreading and fragmenting on a bath of sunflower oil. The initial IPA mass fraction is $\phi_0 = 0.4$, and the volume of the drop is $\Omega_0 = 100$ μL. Methyl blue dye has been added to improve the optical contrast. (b) Sketch of the experiment. The drop of water and alcohol mixture (light gray) spreads over a bath of oil of centimetric depth H. The thickness of the drop $h(r,t)$ depends on time t and on the distance r from the center of the drop. We define the drop radius $R(t)$, the minimal drop thickness h_m, the apparent width d of the peripheral rim, the characteristic velocity V of the flow, and the alcohol fractions ϕ_0 at the center and ϕ_c at the boundary of the drop. j_v is the volume of alcohol evaporated from the drop per unit time and surface area. (c) Evolution of R as a function of time for various initial IPA fractions ϕ_0 and volumes Ω_0. The maximal spreading radius $R_{\max}$ and total experiment time $t_{\exp}$ can be defined on each data set.

When $S > 0$, the drop spreads and reveals a time-dependent thickness profile $h(r,t)$ that we measure using interferometry. We shine white or monochromatic (mercury green, wavelength $\lambda_{Hg} = 546.1$ nm) light with quasinormal incidence from above and observe the reflected fringes of equal thickness. White light patterns provide the absolute thickness h_m of the thinnest parts of the film through a comparison of the interference colors with a Michel-Lévy chart (see Fig. 2 in Supplemental Material, Sec. III [35]). We use this information as a calibration to explore thicker regions whose profiles are inferred from monochromatic interferences. Figure 3(a) shows the time-dependent thickness profiles of a binary drop of IPA mass fraction $\phi_0 = 0.6$ and volume $\Omega_0 = 5$ μL, plotted in the semilog scale. The thickness of the central part of the drop is typically 10 μm, in a circular region of centimetric radius. h decreases progressively toward the periphery and reaches a minimal value h_m a few millimeters away from the drop boundary. h_m is nearly constant during an experiment and is a function of ϕ_0: h_m increases from 70 nm to 1.5 μm as ϕ_0 decreases from 0.8 to 0.4 [see Fig. 2(c) in Supplemental Material [35]]. The outermost part of the drop is a rim which does not exhibit interference fringes due to its strong thickness gradients. The width d of that rim is also a function of ϕ_0 and increases from 30 to 300 μm as ϕ_0 decreases from 0.8 to 0.4.

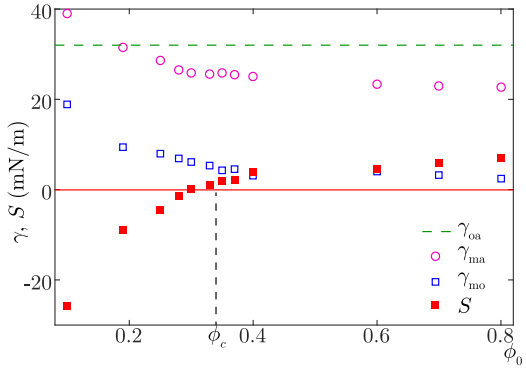

FIG. 2. Measured interfacial tensions: oil-air ($\gamma_{oa} \simeq 32$ mN/m, dashed line), mixture-air (γ_{ma}, open circle), and mixture-oil (γ_{mo}, open square) as a function of the initial IPA mass fraction ϕ_0. The spreading parameter $S = \gamma_{oa} - \gamma_{ma} - \gamma_{mo}$ (filled square) of the mixture on the oil becomes positive for $\phi > \phi_c \simeq 0.35$, the critical IPA fraction above which we observe spontaneous drop spreading and fragmentation [see Fig. 1(a) in Supplemental Material for the plot corresponding to ethanol-water mixtures [35]].

At such small thicknesses, the drop is strongly affected by the evaporation of alcohol, which modifies its local composition. During the spreading of the drop, isopropyl alcohol evaporates much faster than water. Even if evaporation were spatially uniform, the evaporation depletes preferentially the IPA content in the thinnest parts of the drops located near the edge. Evaporation may be even more pronounced at the periphery of the drop as in the case of "coffee rings," which amplifies this effect [2–5]. As a consequence, the spreading parameter progressively decreases toward the edge of the drop, which hinders its spreading and eventually leads to its dewetting. We estimate the evaporation rate by monitoring the weight of a Petri dish filled with mixtures of water and IPA (see Sec. IV in Supplemental Material [35]). The evaporation rates are of the order of 10^{-4} kg/m^2/s, which corresponds to a liquid volume rate of $j_v \simeq 100$ nm/s. With a minimal

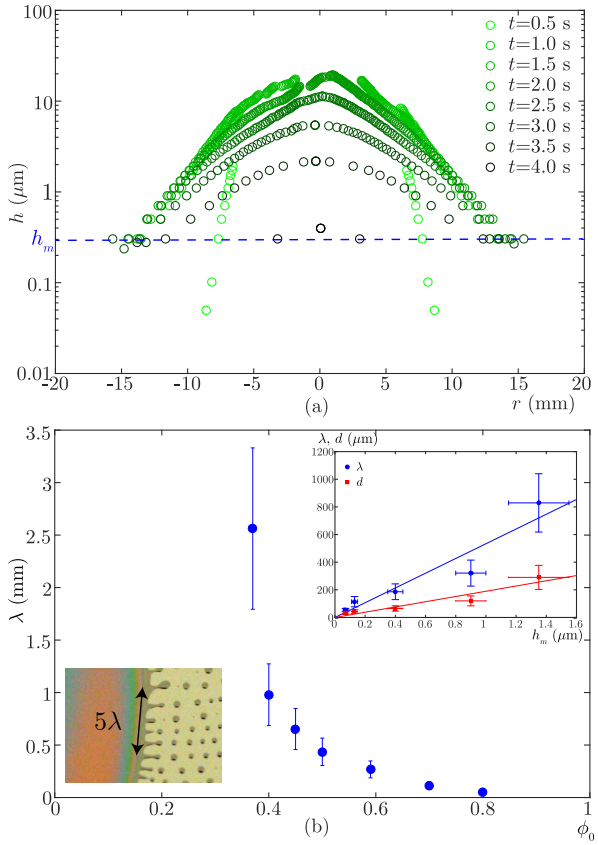

FIG. 3. (a) Thickness profiles $h(r)$ of a drop of volume $\Omega_0 = 5\ \mu$L and IPA fraction $\phi_0 = 0.6$ at successive times in the experiment. The typical thickness is 10 μm, with a thick central region surrounded by a submicron annular base. The dashed line indicates the minimal thickness h_m of the drop close to its periphery. For this experiment, $h_m \simeq 300$ nm. (b) The wavelength λ of the observed instability seems to diverge for $\phi_0 = \phi_c$ and strongly decreases with increasing ϕ_0, concomitantly with the radius of ejected droplets. The inset plot displays the variation of λ and the apparent rim diameter d with the minimal thickness of the film h_m. The lines of equation $\lambda = 533 h_m$ and $d = 190 h_m$ are linear fits to the data.

thickness h_m of a few hundreds of nanometers, most of the alcohol evaporates from the thinnest part of the film within a few seconds. The combination of this estimate with the observation of a finite spreading radius suggests that the composition of the mixture near the edge is close to ϕ_c.

The spatial variations in IPA content result in increasing interfacial tensions toward the edge of the drop. These gradients induce Marangoni tangential stresses at both mixture-air and mixture-oil interfaces, which drive radial flows from the center to the periphery of the drop. As described in Supplemental Material (see Sec. V [35]), we followed the trajectories of chalk particles deposited on the surface of the mixture drop and estimated velocities of the surface flow $V \sim 1$ cm/s. We also used 20 μm diameter polystyrene beads to track the flow in the bath of oil. The characteristic velocity in the bath is comparable to the surface velocity. The observed shear across the thickness of the oil layer indicates that viscous dissipation mainly occurs in the supporting bath.

As a partial conclusion, evaporation imposes dewetting at the edge of the drop and induces an outward Marangoni flow. The combination of these two effects results in the formation of a thicker rim at the periphery of the drop, which becomes unstable. The physical mechanism underlying our experiment is reminiscent of the solutal Marangoni convection observed when a solution of soluble surfactant is continuously injected at the surface of a bath of water [37,38].

Besides dictating the threshold for the overall process, the initial alcohol concentration ϕ_0 also influences the fragmentation mechanism. The drop is bounded by a circular rim which destabilizes into small droplets through a process reminiscent of the classical Plateau-Rayleigh instability of liquid cylinders [1] or other moving contact line instabilities [39,40]. Both the wavelength of the instability λ and the size of the resulting droplets strongly depend on ϕ_0. As a typical variation, λ decays from 2.5 mm to 50 μm as ϕ_0 increases from 0.37 to 0.8, as plotted in Fig. 3(b). We also observe that λ and the characteristic width d of the rim are roughly proportional to the minimal thickness of the film h_m [see the inset in Fig. 3(b)]. The average apparent diameter of the ejected droplets follows the same trend and typically ranges from a few microns to a fraction of a millimeter. This self-emulsification phenomenon thus enables producing droplets whose volume spans about 6 orders of magnitude. Depending on ϕ_0, the fragmentation of a millimetric drop into micron-size fragments may produce up to about 10^7 microdroplets within typically 1 min. The fragmentation mechanism is modified for high concentrations in IPA. For $\phi_0 > 0.7$, holes spontaneously nucleate in several places in the thin film and are advected toward the periphery. Tiny droplets are also released, and the outer boundary of the mother drop appears corrugated (see Supplemental Material, Sec. VI and Movie 4 [35]).

Having presented the main experimental features, we now describe the physical mechanisms at play. Plotting $R/R_{\max}$ versus $t/t_{\exp}$ for different experiments, we observe that all $R - t$ data sets collapse on a single master curve [Fig. 4(a)]. The apparent self-similarity of the spreading dynamics encourages us to describe the problem in terms of scaling laws, and we here propose to derive the characteristic radius and time scale involved in the phenomenon. As the center of the drop is thick, we assume that the volume fraction of alcohol in this region remains equal to ϕ_0. In the vicinity of the edge, the composition of the thin film drops to ϕ_c due to evaporation. The slow evaporation of water is neglected as well as the difference in densities between pure liquids and the mixture.

Our estimate of the flow field suggests that most of the viscous dissipation occurs in the oil layer. More quantitatively, we expect the drop to undergo a plug flow if the condition $\eta_o/H \ll \eta_{\mathrm{mix}}/h$ is fulfilled, where η_o and η_{mix} are

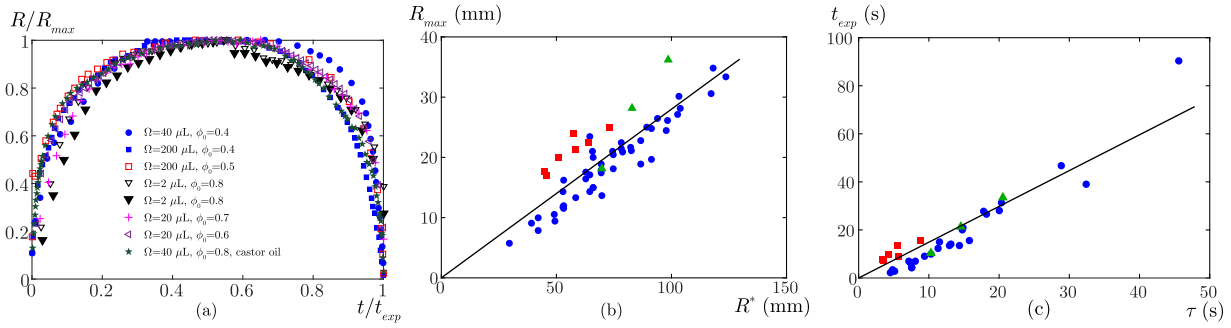

FIG. 4. (a) Normalized plots $R/R_{\max}$ versus $t/t_{\exp}$. Data obtained with drops of different Ω_0 and ϕ_0 and nature of oil (castor oil is about 10 times more viscous than sunflower oil) collapse on a single master curve. (b) Measured spreading radius $R_{\max}$ and (c) duration of the experiment $t_{\exp}$, respectively, as a function of the characteristic radius R^* and time scale τ as predicted by Eqs. (1) and (2). The experimental parameters span the range $0.4 < \phi_0 < 0.8$, $1\ \text{mm} < H < 20\ \text{mm}$, $2\ \text{mm}^3 < \Omega_0 < 500\ \text{mm}^3$. Blue dots (circle) correspond to IPA-water mixtures in a still atmosphere ($j_v = 115\ \text{nm/s}$). Experiments represented by red squares (square) have been performed under a moderate wind ($450\ \text{nm/s} < j_v < 1240\ \text{nm/s}$). Green triangles (triangle) correspond to ethanol-water mixtures in a still atmosphere ($j_v = 130\ \text{nm/s}$). Black lines are linear fits to the data: $R_{\max} = 0.28R^*$ and $t_{\exp} = 1.5\tau$.

the respective viscosities of the oil and of the mixture. In our experiments, $H \sim 5$ mm, $h \lesssim 10\ \mu$m, $\eta_o \simeq 55\ \text{mPa}\cdot\text{s}$, and $0.9 < \eta_{\text{mix}} < 2.3\ \text{mPa}\cdot\text{s}$, which leads to $\eta_o h/\eta_{\text{mix}} H < 0.1$. The spreading drop may thus be viewed as a single interface with an effective tension γ accounting for the contribution of both interfaces: $\gamma = \gamma_{\text{mo}} + \gamma_{\text{ma}}$. γ varies from γ_0 corresponding to the alcohol concentration ϕ_0 at the center of the drop to γ_c at the periphery where the alcohol fraction is ϕ_c. The resulting gradient in surface tension driving the flow is thus of the order of $\Delta\gamma/R^*$, where $\Delta\gamma = \gamma_c - \gamma_0$ and R^* is the characteristic radius of the drop. The flow in the oil develops close to the upper surface from a boundary layer of thickness $\delta(t) \sim \sqrt{\nu t}$, where $\nu \simeq 5 \times 10^{-5}\ \text{m}^2/\text{s}$ is the kinematic viscosity of the oil. For $H \sim 5$ mm, δ reaches H within less than a second, so that the flow is developed across the whole oil layer during most of the experiment: The viscous stress in the oil is thus of the order of $\eta_o V/H$. Balancing tangential stresses at the interface, we deduce the Marangoni-induced flow velocity $V \sim \Delta\gamma H/\eta_o R^*$. The convection of the liquid from the center to the edge defines the time scale of the experiment as $\tau \sim R^*/V$. During this time, a quantity $(\phi_0\Omega_0 - \phi_c\Omega_f) \sim j_v R^{*2}\tau$ of alcohol evaporates, where Ω_0 and Ω_f correspond to the initial and final volume of the drop, respectively. Volume conservation of water imposes $(1-\phi_0)\Omega_0 = (1-\phi_c)\Omega_f$. Combining these relations, we deduce both R^* and τ:

$$R^* \sim \left(\frac{(\phi_0 - \phi_c)\Delta\gamma H\Omega_0}{(1-\phi_c)\eta_o j_v}\right)^{1/4}, \tag{1}$$

$$\tau \sim \left(\frac{(\phi_0 - \phi_c)\eta_o\Omega_0}{(1-\phi_c)\Delta\gamma H j_v}\right)^{1/2}. \tag{2}$$

We measured the maximum spreading radius $R_{\max}$ and the duration $t_{\exp}$ of the experiment for different values of the physical parameters. The agreement with scaling predictions is very good as represented in Figs. 4(b) and 4(c). We obtain $R_{\max} = 0.28(\pm 0.02)R^*$ and $t_{\exp} = 1.5(\pm 0.15)\tau$. Our model thus captures the essential physical mechanisms at play in the phenomenon.

In conclusion, we have shown how a binary mixture of water and alcohol destabilizes as it spreads on a bath of oil. The instability is observed for alcohol concentrations that would lead to a complete spreading of the drop in the absence of evaporation. However, the evaporation of alcohol modifies the wetting properties of the mixture in the vicinity of the spreading front, which quickly stops its progression. Nevertheless, the front does not immediately recede as in classical dewetting [1]. The gradient of alcohol concentration induced by evaporation generates a strong Marangoni flow from the center of the drop to its periphery. This flow feeds an unstable rim that periodically emits tiny droplets whose size is set by the width of the rim. In contrast with other Marangoni instabilities on solid substrates [24–32], the presence of a thick lubricating layer of oil favors high flow velocities and conveys the emitted droplets away. Decreasing the thickness of the oil layer hinders the spreading and the release of droplets. The phenomenon is not observed for $H \lesssim 0.5$ mm. This instability is not limited to the particular case of drops of alcohol-water mixtures deposited on vegetable oils. The same features are obtained with mixtures of perfluorinated ether (methoxy-nonafluorobutane) and perfluorodecalin deposited on a bath of silicone oil (Supplemental Material, Sec. II [35]).

Although our scaling law analysis successfully predicts the spreading radius and the experimental time scale, our global approach does not describe other details of the experiments. For instance, the self-similar shape of the $R(t)$ curve is not captured by this minimal model. Similarly, rescaling the thickness profiles $h(r,t)$ by the maximal thickness of the drop $h_{\max}(t)$ does not lead to a universal

plot (see Supplemental Material, Sec. VII [35]). As in many previous studies on dewetting or bursting films [34,41,42], the formation of the rim and its destabilization into droplets are not yet fully understood. A more refined description accounting for inhomogeneous thickness profiles and velocity fields is challenging but beyond the scope of the present work. We hope that our experimental study will stimulate further theoretical and numerical developments coupling hydrodynamics, Marangoni stresses, wetting, and evaporation. The fragmentation mechanism presented in our study may finally pave the way for practical applications. In a few seconds, two-dimensional assemblies of up to millions of droplets are indeed produced spontaneously, and their volume can be tuned by adjusting the concentration or evaporation rate of the volatile phase.

We are very grateful to Gustavo Gutierrez from Universidad Simon Bolivar, Venezuela, who generously introduced us to this beautiful phenomenon. We warmly thank Guillaume Durey and Hoon Kwon from the Lutetium Project [43] for their support in realizing the Supplemental Movies. We thank Alexey Rednikov and Sam Dehaeck for stimulating discussions and Arthur Meyre for his experimental help. P. C. acknowledges financial support of the Fonds de la Recherche Scientifique—FNRS. This work was partly funded by the Interuniversity Attraction Poles Program (IAP 7/38 MicroMAST) initiated by the Belgian Science Policy Office.

*etienne.reyssat@espci.fr
†jose.bico@espci.fr

[1] P.-G. de Gennes, F. Brochard-Wyart, and D. Quéré, *Capillarity and Wetting Phenomena* (Springer, New York, 2004), ISBN 978-1-4419-1833-8.
[2] R. D. Deegan, O. Bakajin, T. F. Dupont, G. Huber, S. R. Nagel, and T. A. Witten, Nature (London) **389**, 827 (1997).
[3] Y. O. Popov, Phys. Rev. E **71**, 036313 (2005).
[4] J. Park and J. Moon, Langmuir **22**, 3506 (2006).
[5] H. Kim, F. Boulogne, E. Um, I. Jacobi, E. Button, and H. A. Stone, Phys. Rev. Lett. **116**, 124501 (2016).
[6] P. Jiang, J. F. Bertone, K. S. Hwang, and V. L. Colvin, Chem. Mater. **11**, 2132 (1999).
[7] E. Rabani, D. R. Reichman, P. L. Geissler, and L. E. Brus, Nature (London) **426**, 271 (2003).
[8] M. Schnall-Levin, E. Lauga, and M. P. Brenner, Langmuir **22**, 4547 (2006).
[9] L. E. Scriven and C. V. Sternling, Nature (London) **187**, 186 (1960).
[10] S. Nakata, Y. Iguchi, S. Ose, M. Kuboyama, T. Ishii, and K. Yoshikawa, Langmuir **13**, 4454 (1997).
[11] J. W. Bush and D. L. Hu, Annu. Rev. Fluid Mech. **38**, 339 (2006).
[12] F. Domingues Dos Santos and T. Ondarçuhu, Phys. Rev. Lett. **75**, 2972 (1995).
[13] K. Ichimura, Science **288**, 1624 (2000).
[14] S. Daniel, M. K. Chaudhury, and J. C. Chen, Science **291**, 633 (2001).
[15] M. L. Cordero, D. R. Burnham, C. N. Baroud, and D. McGloin, Appl. Phys. Lett. **93**, 034107 (2008).
[16] N. J. Cira, A. Benusiglio, and M. Prakash, Nature (London) **519**, 446 (2015).
[17] H. Hu and R. G. Larson, Langmuir **21**, 3972 (2005).
[18] W. D. Ristenpart, P. G. Kim, C. Domingues, J. Wan, and H. A. Stone, Phys. Rev. Lett. **99**, 234502 (2007).
[19] Y. Tsoumpas, S. Dehaeck, A. Rednikov, and P. Colinet, Langmuir **31**, 13334 (2015).
[20] F. Brochard, Langmuir **5**, 432 (1989).
[21] P. Carles and A. M. Cazabat, in *Surfactants and Macromolecules: Self-Assembly at Interfaces and in Bulk* (Steinkopff, Darmstadt, 1990), Vol. 82, pp. 76–81.
[22] M. Santiago-Rosanne, M. Vignes-Adler, and M. G. Velarde, J. Colloid Interface Sci. **234**, 375 (2001).
[23] E. Saiz and A. P. Tomsia, Nat. Mater. **3**, 903 (2004).
[24] S. M. Troian, X. L. Wu, and S. A. Safran, Phys. Rev. Lett. **62**, 1496 (1989).
[25] A. B. Afsar-Siddiqui, P. F. Luckham, and O. K. Matar, Langmuir **19**, 703 (2003).
[26] A. Hamraoui, M. Cachile, C. Poulard, and A. Cazabat, Colloid Surf. A **250**, 215 (2004).
[27] E. Sultan, A. Boudaoud, and M. Ben Amar, J. Fluid Mech. **543**, 183 (2005).
[28] Y. Gotkis, I. Ivanov, N. Murisic, and L. Kondic, Phys. Rev. Lett. **97**, 186101 (2006).
[29] C. M. Bates, F. Stevens, S. C. Langford, and J. T. Dickinson, Langmuir **24**, 7193 (2008).
[30] R. V. Craster and O. K. Matar, Rev. Mod. Phys. **81**, 1131 (2009).
[31] J. B. Fournier and A. M. Cazabat, Europhys. Lett. **20**, 517 (1992).
[32] A. E. Hosoi and J. W. M. Bush, J. Fluid Mech. **442**, 217 (2001).
[33] H. Gelderblom, H. A. Stone, and J. H. Snoeijer, Phys. Fluids **25**, 102102 (2013).
[34] D. Yamamoto, C. Nakajima, A. Shioi, M. P. Krafft, and K. Yoshikawa, Nat. Commun. **6**, 7189 (2015).
[35] See Supplemental Material at http://link.aps.org/supplemental/10.1103/PhysRevLett.118.074504 for additional data with different systems, interferometry analysis of the thickness of the spreading film, measurements of the evaporation rates, estimates of the velocity fields and local observations of the unstable rim, which includes Refs. [16,36].
[36] D. Vella and L. Mahadevan, Am. J. Phys. **73**, 817 (2005).
[37] M. Roché, Z. Li, I. M. Griffiths, S. Le Roux, I. Cantat, A. Saint-Jalmes, and H. A. Stone, Phys. Rev. Lett. **112**, 208302 (2014).
[38] S. Le Roux, M. Roché, I. Cantat, and A. Saint-Jalmes, Phys. Rev. E **93**, 013107 (2016).
[39] A. L. Bertozzi and M. P. Brenner, Phys. Fluids **9**, 530 (1997).
[40] D. Takagi and H. E. Huppert, J. Fluid Mech. **647**, 221 (2010).
[41] É. Reyssat and D. Quéré, Europhys. Lett. **76**, 236 (2006).
[42] H. Aryafar and H. P. Kavehpour, Phys. Rev. E **78**, 037302 (2008).
[43] https://www.lutetium.paris/en/.